JOURNAL OF PROPULSION AND POWER
Vol. 9, No. 1, Jan.–Feb. 1993

Numerical Analysis of Reacting Flows Using Finite Rate Chemistry Models

Chae M. Rhie*
Pratt and Whitney, United Technologies Corporation, East Hartford, Connecticut 06108
and
Steven T. Stowers† and Houshang B. Ebrahimi‡
Pratt and Whitney, United Technologies Corporation, Palm Beach, Florida 33478

A computational procedure to analyze the reacting flows in supersonic flow regime has been developed. The Navier-Stokes solution algorithm is based on an operator splitting procedure using pressure correction equations. The chemical species solution algorithm is also based on an operator splitting procedure in which the chemical kinetics and the fluid dynamics are solved in separate steps. The predictor step of this chemical kinetics/fluid dynamics coupling procedure, evaluates the effective chemical source terms, by integrating the linearized chemical kinetics equations. The corrector step then solves the fluid dynamic part of the chemical species equations. The present numerical solutions are validated using the available experimental data.

Nomenclature

C_p	=	constant pressure specific heat
f	=	species mass fraction
G_1, G_2, G_3	=	curvilinear velocity components
H	=	total enthalpy including heat of formation
h	=	static enthalpy
J	=	Jacobian in the coordinate transformation
MW_i	=	molecular weight of species
N	=	number of species
NR	=	number of reactions
P	=	static pressure
Pr_l, Pr_t	=	laminar and turbulent Prandtl number
R_0	=	universal gas constant
S	=	source term in finite difference equation
T	=	static temperature
u_i	=	components of Cartesian velocity vector
x_i	=	Cartesian coordinate components
Γ	=	effective diffusion coefficient
δ_{ij}	=	Kronecker delta
κ, ε	=	turbulence kinetic energy and dissipation rate
μ_l, μ_t	=	laminar and turbulent viscosities
ξ, η, ζ	=	curvilinear coordinate components
ρ	=	density
ϕ	=	general transport equation scalar quantity

I. Introduction

IN recent years, the supersonic combustor has drawn revitalized attention as a propulsion device for high-speed vehicles. In this combustor, fuel is injected through parallel and transverse injectors to control fuel mixing and heat release based on the flight speed.

The purpose of the current work is to develop an analytical tool to analyze supersonic combustor flowfields involving chemical reactions between injected hydrogen fuel and a supersonic external stream. In the case of transverse fuel injection, the flow in the vicinity of the fuel injector is highly three-dimensional, turbulent, recirculating, and chemically reacting. These complex flow features necessitate the development of a full three-dimensional viscous flow solver in conjunction with chemical reactions. The present analysis method solves the three-dimensional Reynolds averaged Navier-Stokes equations including transport equations for chemical species.

The present numerical method for the Navier-Stokes equations is based on the operator splitting procedure developed by Rhie and Stowers.[1] In this solution algorithm, a multistep pressure correction procedure is used with an implicit density treatment to establish the pressure and the velocity fields. The equations are implicitly integrated with under relaxation. The current effort is centered around the development of the chemistry coupling procedure within the existing flow solver.

An operator splitting method originally developed by Tyson and Kliegel[2] was used for the coupling of the chemical kinetics with the fluid dynamics. In the predictor step, all the chemical source terms are linearized and implicitly integrated over the residence time for each computational cell. This step simulates the chemical kinetics process and produces effective chemical source terms. In the corrector step, the convection and diffusion parts (i.e., fluid dynamics) of the equations are integrated with the effective chemical source terms from the predictor step.

In the present work, two different hydrogen-air chemistry models were applied. The first one is the global two-reaction finite rate model developed by Rogers and Chinitz[3] and the second one is the detailed eight-reaction finite rate model used in the SCORCH code as described in Refs. 4 and 5.

The global chemistry model uses two reactions and five species. This model replicates the temperature history for the complete chemical reaction mechanism (Ref. 3). Even though this model has restrictions on equivalence ratio and initial temperature, it is considered to produce reasonable engineering information without using extensive computer resources. The detailed chemistry model uses eight reactions and seven species. This model requires more computer resources, but it can describe the chemical reaction mechanism in more detail and relieve some numerical stiffness problems associated with the global model. The benefit of this detailed chemistry model over the global model will be discussed in the present work.

The purpose of the present paper is to describe the present computational procedure and to demonstrate the efficacy of the approach. The results are validated against available experimental data to establish the calibration of the present analytical models for future scramjet applications.

Presented as Paper 89-0459 at the AIAA 27th Aerospace Sciences Meeting, Reno, NV, Jan. 9–12, 1989; received Jan. 26, 1989; revision received May 10, 1990; accepted for publication Jan. 2, 1992.

*Staff Scientist.
†Senior Analytical Engineer. Member AIAA.
‡Senior Analytical Engineer.

II. Mathematical Model

A. Governing Equations

The governing equations for multiple species undergoing chemical reactions are the continuity, Navier-Stokes, energy, and species continuity equations. In generalized tensor notation they can be written:

Continuity

$$\frac{\partial}{\partial x_j}(\rho u_j) = 0 \tag{1}$$

Momentum

$$\frac{\partial}{\partial x_j}(\rho u_i u_j) = -\frac{\partial P}{\partial x_i} + \frac{\partial}{\partial x_j}\left[\mu\left(\frac{\partial u_i}{\partial x_j} + \frac{\partial u_j}{\partial x_i}\right) - \frac{2}{3}\delta_{ij}\mu\frac{\partial u_k}{\partial x_k}\right] \tag{2}$$

Energy

$$\frac{\partial}{\partial x_j}(\rho u_j H) = \frac{\partial}{\partial x_j}\left[\Gamma\frac{\partial H}{\partial x_j} + \frac{1}{2}(\mu - \Gamma)\frac{\partial u_k^2}{\partial x_j}\right] \tag{3}$$

Species Continuity

$$\frac{\partial}{\partial x_j}(\rho u_j f_i) = \dot{\omega}_i + \frac{\partial}{\partial x_j}\left(\mu\frac{\partial f_i}{\partial x_j}\right) \tag{4}$$

where ρ is the density, u the mean velocity, P the pressure, μ the effective viscosity, H the total enthalpy, Γ the effective dissusion coefficient, f_i the mass fraction of chemical species, and $\dot{\omega}_i$, the chemical source term. The unsteady terms are dropped since only steady state solutions are sought in the present study. The transport coefficients for turbulent flow are given by

$$\mu = \mu_l + \mu_t \tag{5}$$

$$\Gamma = (\mu_l/Pr_l) + (\mu_t/Pr_t) \tag{6}$$

where Pr is the Prandtl number. The subscript l denotes the laminary property, and t the turbulent property. The laminar viscosity and conductivity for each of the species are determined using curve fits based on data of Suehla.[6] The turbulent viscosity is determined using the standard High Reynolds number $\kappa - \varepsilon$ two equation turbulence model. Wall functions are used for the near wall regions.

The above equations were derived assuming standard binary diffusion for all species and the effective Lewis number equal unity. For engineering calculation, the simplification of the energy equation with the Lewis equal one, are justified for turbulent flows. For the chemical species equation, Eq. (4), the effective Schmidt number was assumed to be one. It is a good engineering approximation (especially for the near injector flowfield) however, it may lead to insufficient turbulent mixing for the far downstream flowfield. In fact, the turbulent Schmidt number for the far downstream flowfield may have to be about 0.5. The influence of the effective Schmidt number on the far downstream turbulent mixing will be studied in future work.

B. Thermodynamics Model

In addition to the equations described above, expressions are required for the thermodynamic quantities. In the present work, the fluid medium is assumed to be a thermally perfect gas; consequently, the specific heats for all species are function of temperature only. The specific heats can then be calculated using a fourth order polynomial

$$C_p = A_i + B_iT + C_iT^2 + D_iT^3 + E_iT^4 \tag{7}$$

where T is the static temperature and A_i, B_i, C_i, D_i, E_i are curve fit constants based on McBride et al.[7]

The static enthalpy h, is

$$h = \sum_{i=1}^{N} f_i h_i(T) \tag{8}$$

and density is obtained from the equation of state for a multicomponent mixture

$$\rho = \frac{P}{R_0 T \sum_{i=1}^{N} \frac{f_i}{MW_i}} \tag{9}$$

where R_0 is the universal gas constant, and MW_i the molecular weight of species.

In order to determine the equilibrium constants necessary for the finite chemistry models, the gibbs energy is required. For a constant pressure process, the gibbs energy is obtained by

$$g_i/R = A_i(T - T\ln T) - (B_i/2)T^2 - (C_i/6)T^3 - (D_i/12)T^4 - (E_i/20)T^5 + F_i - G_iT \tag{10}$$

where R is a constant and F_i, G_i are additional curve fit constants. The gibbs energy for a reaction can then be obtained

$$\Delta G_R = \sum_{i=\text{products}} n_i g_i - \sum_{i=\text{reactants}} n_i g_i \tag{11}$$

where n is in moles. Finally, the equilibrium constant for each reaction is

$$K_j = \left(\frac{1}{R^{0\prime}T}\right)^{\Delta n} \exp\left(\frac{-\Delta G_R}{R^0 T}\right) \tag{12}$$

where Δn is the difference in moles between products and reactants and $R^{0\prime}$, R^0 are constants.

C. Finite Rate Chemistry Models

For the present scramjet combustor simulation study, two different finite rate chemistry models for gaseous hydrogen and air have been selected. The first one is the global two-reaction finite rate model described in Rogers and Chinitz[3] and the second one is the detailed eight-reaction finite rate model as described in Ref. 5.

1. *Two-Step Reaction Model*

This model was deduced from results obtained with a 28-reaction mechanism employed in a series of one-dimensional, constant-pressure, stream-tube calculations (Ref. 3). Even though this model has limitations in the applicable pressure and temperature ranges, it produces reasonable accuracy and the overall nature of the reaction for engineering purposes. The proposed two-step global model is as follows:

$$H_2 + O_2 = 2OH$$

$$2OH + H_2 = 2H_2O$$

The first reaction controls the reaction of the fuel and oxidizer species through the ignition delay period, whereas the second reaction predominates during the combustion phase when the major heat release and product formation occur. The reaction rates can be found in Ref. 3. In the present work, an equilibrium assumption was made for the first reaction. One of the purposes of the present study is to investigate the performance of this model compared to the more detailed eight-reaction model to be explained in the next section.

Table 1 Detailed eight-reaction finite rate model

Reaction number	Reaction rate variables			
	Reaction	A	N	E
1	$OH + O = H + O_2$	3.0E-1	0.0	0.96
2	$OH + H = H_2 + O$	1.4E-14	−1.0	0.7
3	$OH + OH = H_2O + O$	1.0E-11	0.0	1.1
4	$OH + H_2 = H_2O + H$	3.5E-11	0.0	5.18
5	$2H + M = H_2 + M$	3.0E-30	1.0	0.0
6	$H + O + M = OH + M$	1.0E-29	1.0	0.0
7	$2O + M = O_2 + M$	3.0E-34	0.0	−1.8
8	$H + OH + M = H_2O + M$	1.0E-25	2.0	0.0

2. Eight-Step Reaction Model

This model utilizes eight reactions and seven species as shown in Table 1. All of the species H_2, O_2, H_2O, OH, H, O, HO_2, H_2O_2 are considered to be reactive while N_2 is treated as an inert species. The forward rate coefficients for each of the reactions are given by the modified Arrhenius law

$$K_{fj} = A_j T^{-N_j} \exp(-E_j/RT) \tag{13}$$

and the reverse rate is obtained using

$$K_{bj} = K_{fj}/K_j \tag{14}$$

where K_j is the equilibrium coefficient that is determined from Eq. (12)

The production rates for each of the species (chemical source terms) for both chemistry models which are required in Eq. (4) are obtained using the laws of mass action. For a general homogeneous chemical reaction, which may proceed in both the forward and reverse directions, the stoichiometric equation can be written as

$$\sum_{i=1}^{N} \nu'_{ji} \Lambda_i \underset{k_b}{\overset{k_f}{\rightleftarrows}} \sum_{i=1}^{N} \nu''_{ji} \Lambda_i, \qquad j = 1, 2, \ldots, NR \tag{15}$$

The law of mass continuity states that for net production of species i by reaction j is

$$\left(\frac{dC_i}{dt}\right)_j = (\nu''_{ij} - \nu'_{ij}) \left[k_{fj} \prod_{i=1}^{N} C_i^{\nu'_{ij}} - k_{bj} \prod_{i=1}^{N} C_i^{\nu''_{ij}} \right] \tag{16}$$

where C_i is the concentration of species. The net rate of change in concentration of species i by all reactions is found by summing the contribution from each reaction giving

$$\frac{dC_i}{dt} = \sum_{j=1}^{NR} \left(\frac{dC_i}{dt}\right)_j \tag{17}$$

III. Solution Method

A. Solution of Navier-Stokes Equations

The governing equations are transformed to an arbitrary curvilinear coordinate system using the general transform

$$\xi = \xi(x, y, z)$$
$$\eta = \eta(x, y, z)$$
$$\zeta = \zeta(x, y, z) \tag{18}$$

where ξ, η, ζ are the arbitrary curvilinear coordinates, and x, y, z, are the Cartesian coordinates. Applying Gauss's theorem, Eqs. (1–4) can be written in the generalized form

$$(1/J)[(\rho G_1 \phi)_\xi + (\rho G_2 \phi)_\eta + (\rho G_3 \phi)_\zeta] = (1/J)[(J\Gamma\alpha_1\phi_\xi)_\xi + (J\Gamma\alpha_2\phi_\eta)_\eta + (J\Gamma\alpha_3\phi_\zeta)_\zeta + S] + S^\phi \tag{19}$$

where G_1, G_2, and G_3 are the contravariant velocities scaled by the Jacobian J, and ϕ represents the dependent variables (u, v, w, etc.). Equation (19) is then integrated over an arbitrary control volume using a cell center (nonstaggered) grid arrangement. The resulting discretization produces a second order accurate centered differencing. The shocks are effectively captured using the MADE (monotonically adaptive dissipation at extrema) scheme[1,8] in which a flux limiter concept is employed.

The solution procedure for the Navier-Stokes equations are based on the previously developed pressure based method.[1,9] This method is based on an operator splitting concept, to solve the momentum and the continuity equations in separate steps, by means of pressure corrections. In the predictor step, a preliminary velocity field is first obtained from the momentum equations with a preliminary pressure field. Since this preliminary velocity field does not satisfy the continuity equation, pressure correction equations are solved in the corrector step to establish new velocity and pressure fields, which must satisfy the continuity equation. The momentum and the continuity equations are coupled through this pressure correction procedure. The resulting algebraic equation systems are solved implicitly with a multigrid correction scheme.[9]

B. Solution of Chemical Species Equations

In reacting flow problems, a coupled implicit solution procedure of the chemical kinetics/fluid dynamics problem, would require the inversion of a complex system of matrices. The various chemical species are related to each other through the chemical reactions at each grid point, and each species is influenced by neighboring grid points through the fluid dynamics. To avoid the complexities of the $N \times N$ block tridiagonal inversion, the chemical kinetic and the fluid dynamic solutions are uncoupled in performing the integration using an operator splitting concept.

To explain this procedure in more detail, let the governing species continuity equations be written of the form

$$\rho \frac{\partial f_i}{\partial t} = Cf_i + Df_i + \dot{\omega}_i \tag{20}$$

where f_i is the mass fraction of species i, C and D are convective and diffusion operators respectively, and $\dot{\omega}_i$ is the chemical source term for species i.

In the predictor step, the chemical kinetics solution involves integrating the relation

$$\rho \frac{df_i}{dt} = \dot{\omega}(f_1, f_2, \ldots, f_n) \tag{21}$$

in a fully implicit fashion. The fluid dynamic time scale determined by

$$\Delta t = [(U/\Delta x) + (V/\Delta y)]^{-1} \tag{22}$$

where U, V are the Cartesian velocity components, and Δx, Δy, the Cartesian grid spacings, are utilized for the chemical integration step. The two body and three body reactions in Eq. (21) are linearized using the approach of Tyson and Kliegel[2] to establish a simultaneous $N \times N$ algebraic linear matrix as follows:

$$(f_i f_j)^n = -(f_i f_j)^n + (f_j)^o f_i^n + (f_i)^o f_j^n \tag{23}$$

$$(f_i f_j f_k)^n = -2(f_i f_j f_k)^o + (f_j f_k)^o f_i^n + (f_i f_k)^o f_j^n + (f_i f_j)^o f_k^n \tag{24}$$

where superscript n denotes the new time value, and o, the old time value. The resulting $N \times N$ algebraic system can be easily solved. The effective chemical source terms are then determined by dividing the increment of the chemical species by the residence time Eq. (22).

In the corrector step, the convection and the diffusion part of the species equations are implicitly integrated. The corrector step integrates the fluid dynamic part with the effective chemical source terms from the predictor step as follows:

$$Cf_i + Df_i = \left(\rho \frac{\partial f_i}{\partial t}\right)_{\text{eff}} = \rho \frac{\Delta f_i}{\Delta t} \tag{25}$$

where Δf_i is the increment obtained by subtracting the old time value, f_i^o, from the new time value, f_i^n.

IV. CRAY-XMP Computer

A CRAY-XMP 28 computer that has eight mega words maximum core memory is used for the present calculations. The present NASTAR (NAvier-STokes analysis for Arbitrary Regimes) computer code has been fully vectorized and uses the SSD (solid state disk) device for out-of-core calculations. The present out-of-core solution technique stores only three streamwise computational planes at a time in-core, because the influence coefficients resulting from the second order centered discretization require only three grid nodal values. The in-core indices for the three computational planes are rotated like a permutation to avoid data swaps. The resulting matrices are solved using the ADI multigrid scheme in core. As a result, the convergence history is identical to the full in-core calculation. This approach requires nine three-dimensional variables to be stored in the core. The frequency of data transfer to SSD for a variable is about five times/iteration. The I/O wait time due to the use of SSD is less than 10% of the whole computation time. The average computer time for a case to converge is about 10 h/1000 iterations/200,000 grid points with the 2-reaction model. The computational time increases by 35% with the 8-reaction model.

V. Results and Discussion

A careful calibration of the present NASTAR code has been executed to establish a confidence level in future scramjet flow simulations. Several different checks were made. First, one-dimensional premixed fuel injection cases were calculated to check out the chemical kinetics models. Second, two-dimensional tangential fuel injection with turbulence mixing cases were calculated. The results were compared with experimental data. Third, three-dimensional test cases with sonic transverse fuel injections were calculated to check out the jet penetration and spreading rates.

It should be stated that the present work does not fully address the grid independency issue, mainly due to the computer resource limitations, particularly in three-dimensional calculations. During the calculations, the global conservation for each scalar variable was monitored, and the convergence was defined when all the global conservation errors dropped below 0.1%, when normalized by the global inlet scalar fluxes.

A. One-Dimensional Test Cases

One-dimensional premixed fuel injection cases were calculated using three different chemical reaction models: 1) one-reaction, 2) two-reaction, and 3) eight-reaction finite rate models. The eight-reaction model should be considered to be more accurate in this comparative numerical study. The one-reaction model simply used a global

$$2H_2 + O_2 = 2H_2O$$

reaction with reaction rates roughly tuned for low-temperature application. The inlet flow conditions tested were with static pressure, P_∞ = 101,325 Pa, velocity U_∞ = 2689 m/s, and two different static temperatures T_∞ = 1000 and 2000 K.

Figure 1a shows the temperature rise in the first test case in which the inlet static temperature was 1000 K. In this case, the two-reaction model described the ignition delay reasonably well, compared to the eight-reaction model, because the intermediate species in the two-reaction model partially oxidated in the ignition delay period. The one-reaction model could not describe any ignition delay. It appears that the intermediate species was a crucial item for a reasonable combustor simulation in a low temperature rane (1000–2000 K). The result represented by symbols was obtained by Bittkers one-dimensional chemical kinetics code using the eight-reaction model. The difference between the present NASTAR eight-reaction result and the Bittkers result was not well understood.

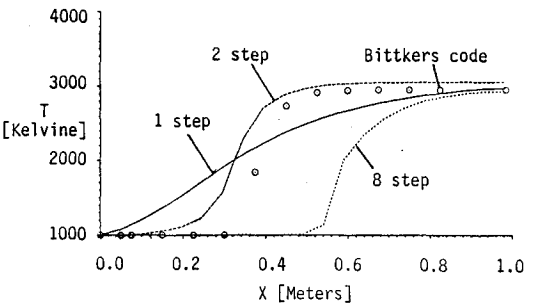

Fig. 1a One-dimensional case (T_∞ = 1000 K).

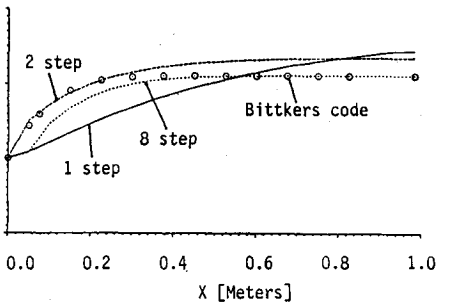

Fig. 1b One-dimensional case (T_∞ = 2000 K).

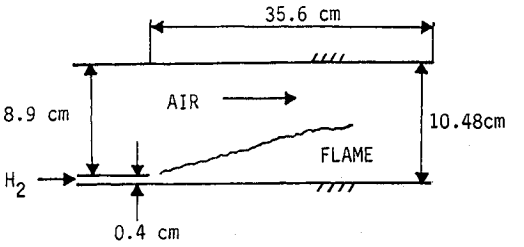

	H2 Jet	Main Stream
M	1.0	2.44
T, (k)	254	1270
U, (M/S)	1216	1764
P, (MPa)	0.1	0.1

Fig. 2 Two-dimensional case by Burrow and Kurkov.[10]

Figure 1b shows the static temperature rise in the second test case in which the inlet static temperature was 2000 K. In this case, the two-reaction model compared well with the eight-reaction model. However, the exit temperature was slightly overpredicted. The one-reaction model showed a slower temperature rise. The slight delay at the inlet in the present NASTAR eight-reaction calculation was due to the large grid spacing which gave overshoots in chemical source terms. A total of 20 equally spaced grid points were used in the present one-dimensional calculation.

B. Two-Dimensional Test Cases

Two-dimensional flows with tangential fuel injections were calculated using two-reaction and eight-reaction models.

The first case was the two-dimensional case tested by Burrows and Kurkov.[10] The geometry and inlet conditions are illustrated in Fig. 2. In this case, a sonic jet of hydrogen was

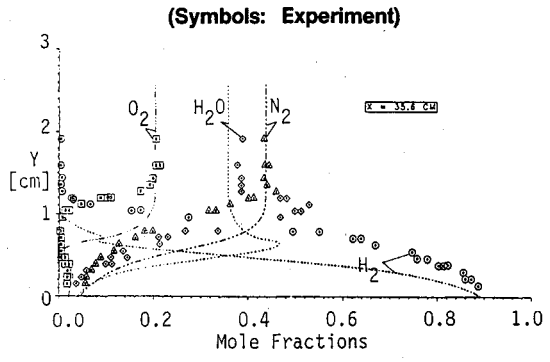

Fig. 3 Chemical species profiles at x = 35.6 cm.

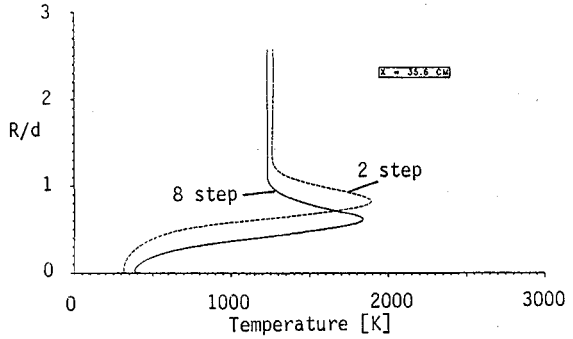

Fig. 4 Static temperature profiles at x = 35.6 cm (2-step with modified reaction).

injected tangentially into a Mach 2.44 vitiated airstream in a near-parallel wall. The airstream had a thick boundary layer that was about three times the size of the initial H_2 jet (0.4 cm). The calculated chemical composition profiles at 35.6 cm using the eight-reaction model is compared with experimental data in Fig. 3. The main difference is that the experimental profiles appear to be shifted away from the wall, even though the shapes of the profiles are in good agreement with the experimental data. It is possible that the present eight-reaction finite rate chemistry missed the ignition in the lean mixture region, or the high effective Schmidt number used in the present study (=1.0) could not enhance enough turbulent mixing in the numerical simulation. An additional calculation was made using the two-reaction model to compare with the eight-reaction model result. Initially, the two-reaction model gave very little reaction. It under-predicted the reaction at this low mainstream temperature (T_∞ = 1270 K). In an effort to generate the reasonable reaction, the static temperatures had to be raised arbitrarily by 250° R during the reaction rate calculation. Figure 4 compares the static temperature profiles at x = 35.6 cm. The chemical species profiles are not compared here, since the two-reaction model was not designed to predict chemical species, but to predict global heat release rates.

The second case was the axisymmetric case tested by Henry and Beach.[11] In this case, cold hydrogen (T = 251 K) of Mach 2.0 was injected along the axis of a circular supersonic stream of hot vitiated air (T_∞ = 1485 K) as shown in Fig. 5. Figure 6 compares predictions of H_2, O_2, and H_2O mass fractions using the eight-reaction with experimental data at x/d_j = 27.9. As can be seen from this figure, the prediction agreed reasonably well with the experimental data. However, a disagreement of the oxygen concentration existed between the calculated and measured values. This indicated that there was an ignition delay in calculation. An additional calculation was also performed for this case using the two-reaction model. This two-reaction model result (Fig. 7) showed a more favorable comparison with the eight-reaction model result than the previous two-dimensional test case (see Fig. 4). One reason for this better agreement may be due to the higher mainstream temperature (T_∞ = 1485 K).

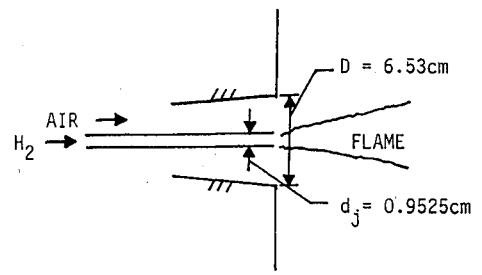

	H2 Jet	Main Stream
M	2.0	1.90
T, (k)	251	1495
U, (M/S)	2432	1510
P, (MPa)	0.1	0.1

Fig. 5 Axisymmetric case by Henry and Beach.[11]

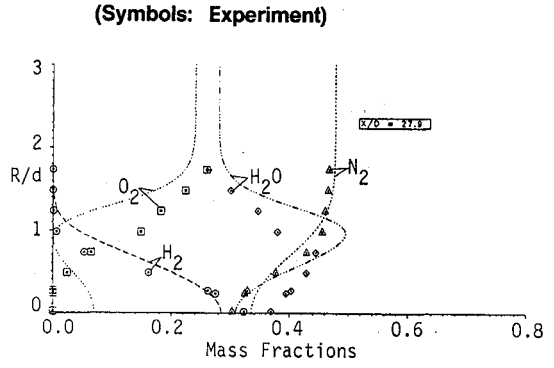

Fig. 6 Chemical species profiles at x/d_j = 27.9.

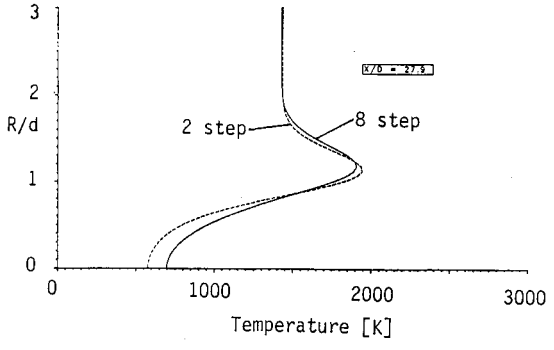

Fig. 7 Static temperature profiles at x/d_j = 27.9.

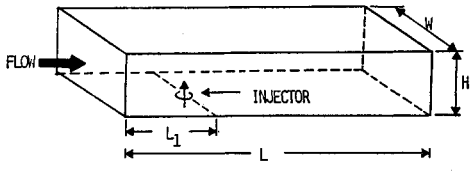

Diameter of Injector (d) = 0.002 m
H/d = 9, L/d = 35, L1/d = 10, W/d = 14

Fig. 8 McDaniels single jet injection case.

C. Three-Dimensional Test Cases

Two normal injection cases were calculated to simulate scramjet combustor flowfields. The problem consisted of a sonic fuel injection into a supersonic freestream of air. The first test case was the nonreacting case (sonic air injection) measured by McDaniel and Graves.[12] Figure 8 shows the geometry and the flow conditions (Table 2). Figure 9 shows a view of the 70 × 50 × 35 grid and the grid detail near the

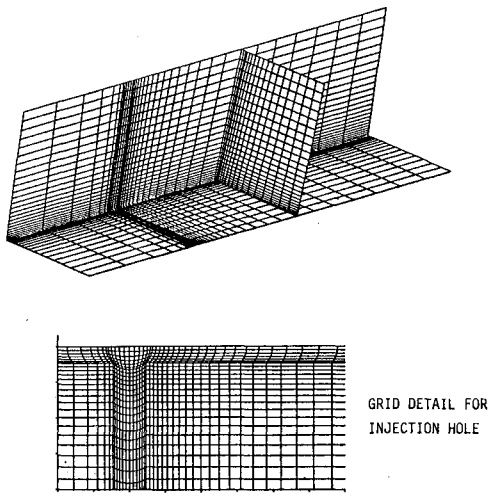

Fig. 9 Computational grid (70 × 50 × 35).

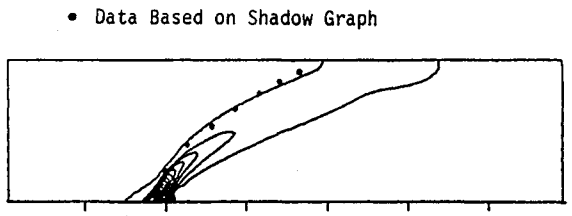

Fig. 10 Pressure ratio contours (P/P_∞) at the symmetry plane.

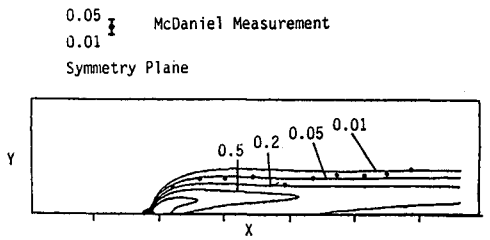

Fig. 11a Mass concentration penetration rate.

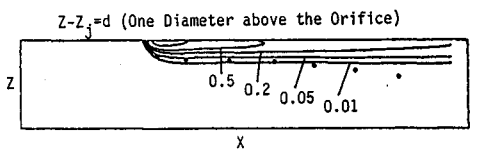

Fig. 11b Mass concentration spreading rate.

Table 2 Flow condition for nonreacting case

	Air jet	Main stream
M	1.0	2.06
T, k	240	170
P, MPa	0.152	0.036

Table 3 Flow condition for reacting case

	H_2 jet	Main stream
M	1.0	4.0
T, k	700	1300
P, MPa	1.6	0.1

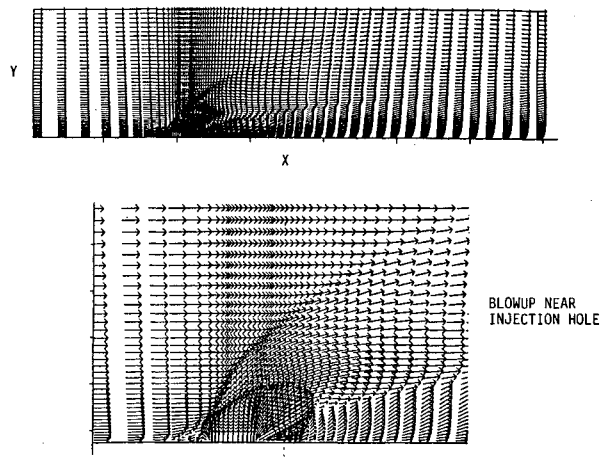

Fig. 12 Velocity vector plots at the plane.

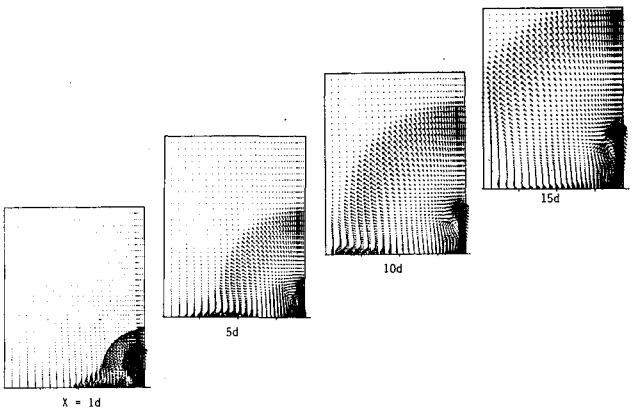

Fig. 13 Velocity vector plots at cross-stream planes.

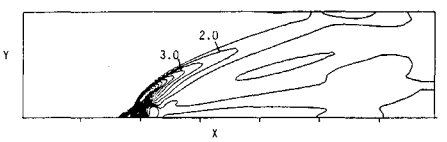

Fig. 14 Pressure ratio contours (P/P_∞) at the symmetry plane.

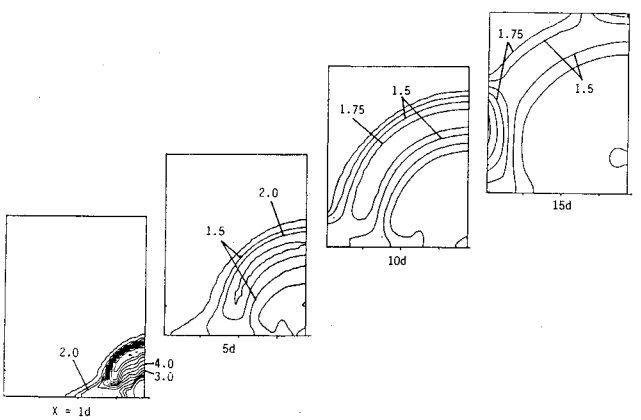

Fig. 15 Pressure ratio contours at cross-stream planes.

injection hole. The constant static pressure contours at the plane of symmetry compared well with shadow graph data as shown in Fig. 10. The constant mass fraction contours at the plane of symmetry in Fig. 11a show good correlations with the measured penetration rate into the external stream. The constant mass fraction contours at 1 diameter above the orifice in Fig. 11b show a somewhat weaker spreading rate compared to the measurement.

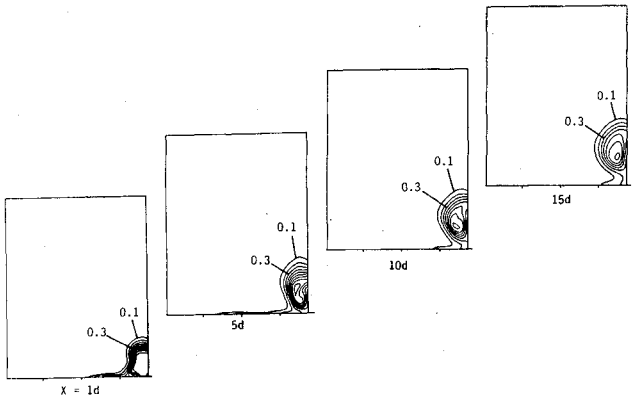

Fig. 16 H_2 mass fraction contours at cross-stream planes.

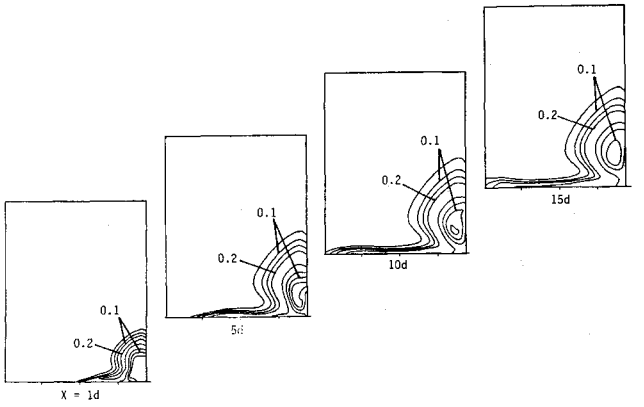

Fig. 17 H_2O mass fraction contours at cross-stream planes.

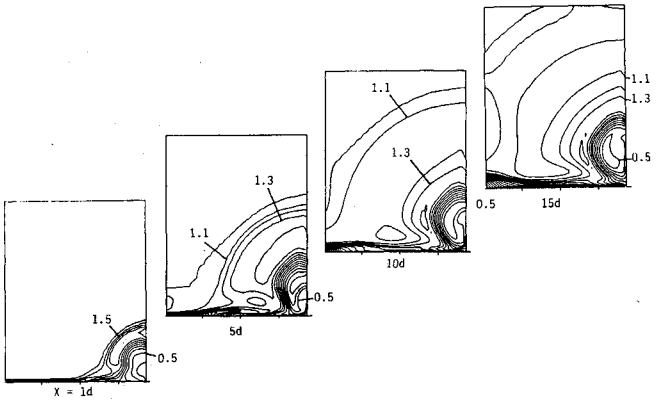

Fig. 18 Static temperature ratio contours (T/T_∞) at cross-stream planes.

The next calculation was performed with a hydrogen injection to simulate a reacting situation. The 8-reaction finite rate model was used. The same geometry as the above nonreacting case was used, but the flow conditions were changed as shown in Table 3. The velocity vectors at the plane of symmetry of the duct are shown in Fig. 12. A complex three-dimensional pattern near the hole is evident (including reversed flow regions). The velocity vectors at different cross-stream planes are shown in Fig. 13. The shock propagation and a reflection from a side wall is clearly visible. A pair of counter rotating votices are also visible downstream of the injection hole (only half the domain is shown in Fig. 13). The static pressure contours at the plane of symmetry and the cross-stream planes are plotted in Figs. 14 and 15. The H_2 mass fraction countours are plotted in Fig. 16. The H_2O production and the static temperature profiles at the different cross-stream planes are plotted in Figs. 17 and 18. Because there are no experimental data available, this case could not

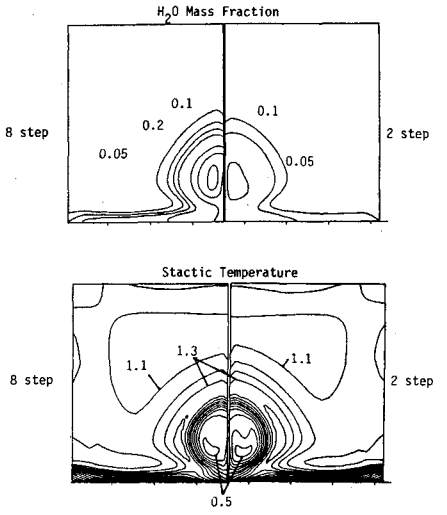

Fig. 19 H_2O mass fraction and static temperature ratio contours at $x = 20$.

be validated, but this simulation was used to study the flow characteristics. An additional calculation was made with the 2-reaction model. The H_2O mass fractions and static temperature predictions at $x = 20d$ location is compared with the 8-reaction calculation in Fig. 19. Even though the static temperature shows reasonable comparison, the H_2O production was under-predicted in the 2-reaction calculation.

VI. Summary

An existing pressure-based Navier-Stokes solver has been extended and validated for chemically reacting flows in a scramjet combustor. The emphasis of the present work was centered around the implementation of the chemical species equations into the existing Navier-Stokes solver (NASTAR code). The chemical kinetics/fluid dynamics coupling was achieved by using an operator splitting concept.

Global and a detailed chemistry models were applied to benchmark cases to establish the calibration of the present analysis method in scramjet applications.

The global 2-reaction model produced reasonable results at high temperatures, but under-predicted reactions at lower temperatures. The detailed 8-reaction model produced reasonable predictions in all temperature ranges, but required more computer resources. It seems that the most critical need in the current CFD calibration phase is an establishment of good three-dimensional experiments.

References

[1]Rhie, C. M., and Stowers, S. T., "Navier-Stokes Analysis for High Speed Flows Using a Pressure Correction Algorithm," AIAA/SAE/ASME/ASEE 23rd Joint Propulsion Conf., AIAA Paper 87-1980, San Diego, CA, June 29–July 2, 1987.

[2]Tyson, R. J., and Kliegel, J. R., "An Implicit Integration Procedure for Chemical Kinetics," AIAA Paper 68-180, Jan. 1968.

[3]Rogers, R. C., and Chinitz, W., "Using a Global Hydrogen-Air Combustion Model in Turbulent Reacting Flow Calculations," *AIAA Journal*, Vol. 21, Jan. 1983, pp. 586–592.

[4]Mikatarian, R. R., Kau, C. J., and Pergament H. S., "A Fast Computer Program for Nonequilibrium Rocket Plume Predictions," AFRPL-TR-72-94, Aug. 1972.

[5]Sinha, N., and Dash, S. M., "Parabolized Navier-Stokes Analysis of Ducted Turbulent Mixing Problems With Finite Rate Chemistry," AIAA Paper 86-0004, Jan. 1986.

[6]Suehla, R. A., "Estimated Viscosities and Thermal Conductivities of Gases at High Temperatures," NASA TR R-132, 1962.

[7]McBride, B. J., Heimel, S., Ehlers, J. G., and Gordon, S., "Thermodynamic Properties to 6000 K for 210 Substances Involving the First 18 Elements," NASA SP-3001, 1963.

[8]White, J. A., and Rhie, C. M., "Numerical Analysis of the Peak Heat Transfer Rate for Hypersonic Flow of a Cowl Leading Edge," AIAA Paper 87-1895, San Diego, CA, 1987.

[9]Rhie, C. M., "A Pressure Based Navier-Stokes Solver With the Multigrid Method," AIAA 23rd Aerospace Sciences Meeting, Jan. 1986, AIAA Paper 86-207, Reno, NV; *AIAA Journal* (to be published).

[10]Burrow, M., and Kurkov, A. P., "Analytical and Experimental Study of Supersonic Combustion of Hydrogen in a Vitiated Airstream," NASA TMV-2828, Sept. 1973.

[11]Henry, J., and Beach, H. L., "Hypersonic Air Breathing Propulsion Systems," NASA SP-292, Paper 8, Nov. 1971.

[12]McDaniel, J. C., and Graves, J., Jr., "A Laser-Induced Fluorescence Visualization Study of Transverse, Sonic Fuel Injection in a Nonreacting Supersonic Combustor," AIAA-86-0507, Reno, NV, Jan. 1986.